

Do regions outside the tropical Pacific influence ENSO through atmospheric teleconnections?

H. Dayan · T. Izumo · J. Vialard · M. Lengaigne · S. Masson

Received: 12 June 2014 / Accepted: 9 July 2014 / Published online: 5 August 2014
© Springer-Verlag Berlin Heidelberg 2014

Abstract This paper aims at identifying oceanic regions outside the tropical Pacific, which may influence the El Niño Southern Oscillation (ENSO) through interannual modulation of equatorial Pacific winds. An Atmospheric General Circulation Model (AGCM) 7-members ensemble experiment forced by climatological sea surface temperature (hereafter, SST) in the tropical Pacific Ocean and observed interannually varying SST elsewhere produces ensemble-mean equatorial zonal wind stress interannual anomalies (ZWSA) over the equatorial Pacific. These ZWSA are largest during boreal winter in the western Pacific, and induce a ~ 0.5 °C response in the central Pacific during the following spring in a simple ocean model, that weakly but significantly correlates with the following ENSO peak amplitude. When correlated with global SST, the residual western equatorial Pacific ZWSA yield SST patterns that are reminiscent of ENSO teleconnections in the Indian, North and South Pacific, and Atlantic Oceans. We further design 20-members ensemble sensitivity experiments forced by typical SST patterns of the main climate modes for each of these regions, in order to identify regions that influence equatorial Pacific ZWSA most. In our experiments, only the Indian Ocean Basin-wide SST warming in late boreal winter produces a statistically significant ZWSA in the western equatorial Pacific, resulting in a weak but significant ~ 0.35 °C SST response in the central Pacific (i.e. ~ 35 % of the observed standard deviation) during the

following spring, the season when the Bjerknes coupled feedback is particularly efficient. This paper hence agrees with previous studies, which suggest that ENSO-induced basin-wide SST signals in the Indian Ocean may contribute to the phase transition of ENSO. Our results suggest that studies exploring external influences on ENSO should adopt a global approach rather than focus on a specific region. Designing coupled model simulations would also allow investigating air–sea interactions-mediated teleconnection mechanisms, which we can't reproduce in our forced AGCM framework.

Keywords El Niño Southern Oscillation · External forcing · Atmospheric teleconnections · Indian Ocean

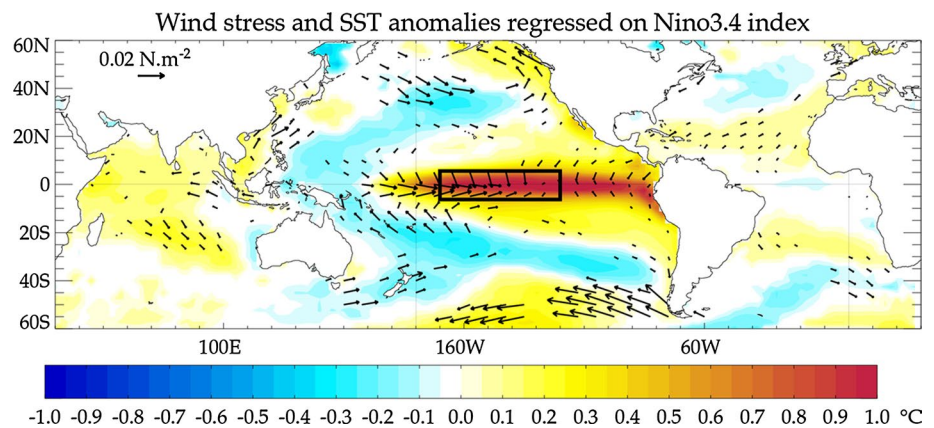
1 Introduction

The El Niño-Southern Oscillation (hereafter ENSO) is the major mode of earth's climate variability at inter-annual timescales (e.g. McPhaden et al. 2006; Deser et al. 2010) with massive socioeconomic impacts. Its positive phase (El Niño) is characterized by warm sea surface temperature anomalies (hereafter, SSTA) in the central and eastern tropical Pacific associated with enhanced deep atmospheric convection and westerly wind anomalies in the western and central Pacific (Fig. 1). These SSTA usually appear in spring and amplify under the effect of the Bjerknes feedback (Bjerknes 1969), a positive air–sea feedback loop in the tropical Pacific. In this positive feedback loop, a positive SSTA in the central Pacific promotes enhanced deep atmospheric convection and an associated westerly wind anomaly (Gill 1980). This wind anomaly drives an anomalous eastward flow in the central Pacific that pushes the warm pool eastward, hence reinforcing the initial SSTA

H. Dayan · T. Izumo · J. Vialard (✉) · M. Lengaigne · S. Masson
CNRS-IRD-MNHN, LOCEAN Laboratory, IPSL, Sorbonne
Universités (UPMC, Univ Paris 06), Paris, France
e-mail: jv@locean-ipsl.upmc.fr

M. Lengaigne
IISc-NIO-IITM-IRD Joint International Laboratory,
NIO, Indo-French Cell for Water Sciences, Dona Paula, India

Fig. 1 Regression coefficient of global monthly ERA-I SST (colours) and wind stress (vectors) anomalies on the Nino3.4 index (SST anomalies averaged over the 170°W–120°W; 5°S–5°N box indicated in black). The regression coefficients are computed over the 1979–2009 period. Only regression coefficients that are significantly different from zero at the 95 % confidence level are plotted



(e.g. Picaut et al. 1996; Vialard et al. 2001). This eventually leads to the development of an El Niño event, usually peaking towards the end of the calendar year.

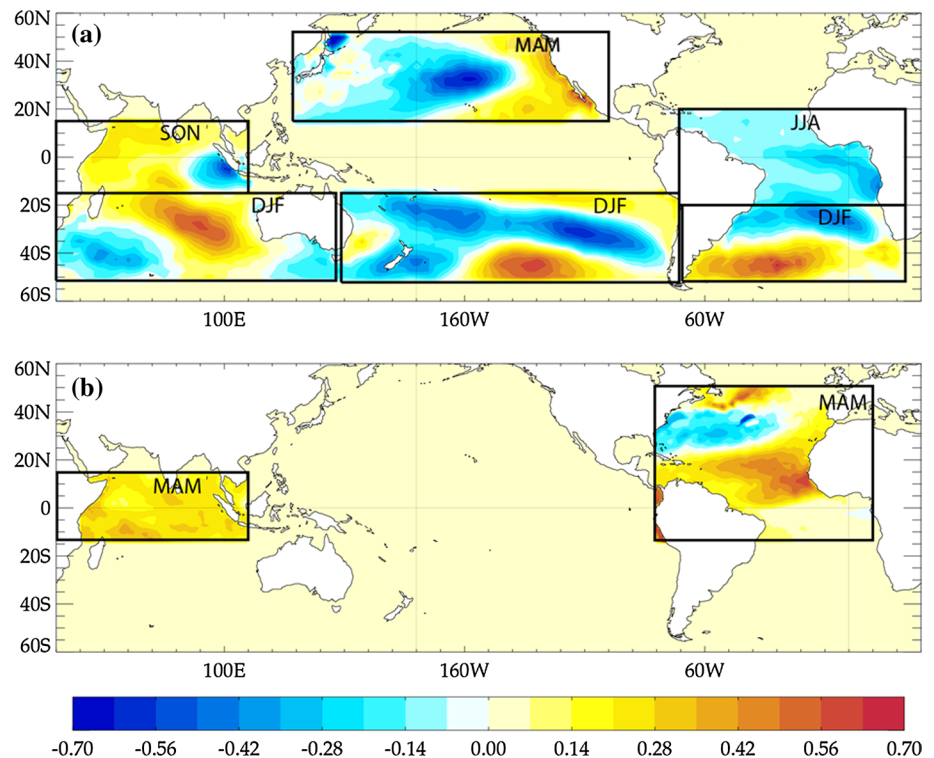
These ENSO-induced changes in deep atmospheric convection in the central Pacific have worldwide climatic impacts through atmospheric teleconnections (e.g. Trenberth et al. 1998). Within the tropics, most of the ENSO remote impacts occur through shifts of the Walker circulation. For example, the eastward shift of the Walker circulation during an El Niño induces anomalous subsidence, increased surface solar heat flux and reduced surface wind over the Indian Ocean. As a result, the entire Indian Ocean basin warms during an ENSO (Fig. 1; Klein et al. 1999; Ohba and Ueda 2005; Xie et al. 2009). The heat source in the central Pacific also induces a stationary planetary-wave response, which is channelled towards the subtropics by waveguides resulting from the mean atmospheric circulation (e.g. Trenberth et al. 1998). This modifies the probability of occurrence of large-scale weather patterns such as the Pacific-North-American (PNA) and North Atlantic Oscillation (NAO) patterns (e.g., Trenberth and Hurrell 1994; Alexander et al. 2002; Newman et al. 2003; Deser et al. 2010). The resulting changes in surface wind (Fig. 1) and heat fluxes force large-scale SSTA in these extra-tropical regions (see for example the characteristic “horseshoe” pattern on Fig. 1). ENSO hence influences oceanic and atmospheric variability at global scale, with sizable societal consequences (McPhaden et al. 2006; Glantz 2001). This is a strong incentive to better understand its possible precursors, and to ultimately improve its prediction.

ENSO is a climate mode that emerges from internal dynamics of the ocean–atmosphere coupled system in the tropical Pacific, with climate impacts at an almost global scale. While there is a clear influence of ENSO on SSTA and related teleconnections at a global scale (e.g. Spencer et al. 2004), several studies have also proposed that SSTA in several regions outside of the tropical Pacific may influence ENSO (e.g. Vimont et al. 2001, 2003, 2009; Meehl et al. 2003; Clarke and Van Gorder 2003; Behera and

Yamagata 2003; Annamalai et al. 2005; Kug and Kang 2006; Ohba and Ueda 2007; Rodríguez-Fonseca et al. 2009; Jansen et al. 2009; Izumo et al. 2010; Ding et al. 2012; Frauen and Dommengot 2012; Martin-Rey et al. 2012; Izumo et al. 2014; Dayan et al. 2013). The general concept of these studies is that anomalies in a given region (e.g. the equatorial Indian Ocean) can induce wind changes over the equatorial Pacific Ocean through atmospheric teleconnections. These wind changes induce an equatorial Pacific SST response, which can further be amplified by the Bjerknes feedback, and interfere with the ENSO cycle. Below, we provide a more detailed review of these studies, based on Fig. 2, that shows the various SST patterns for which past studies suggest an influence on ENSO. The SST patterns on Fig. 2 have been obtained from the leading mode of an empirical orthogonal function (EOF) analysis applied in each sub-region (black frames) for a given season (indicated in the frames).

There are two main modes of interannual SST variability in the tropical Indian Ocean. As described above, the first one is a uniform warming (during El Niños) or cooling (during La Niñas). It is primarily driven by nebulosity changes resulting from anomalous subsidence or ascendance associated with zonal shifts in the Walker circulation (Klein et al. 1999; Ohba and Ueda 2005; Xie et al. 2009). As a result, the entire tropical Indian Ocean warms in response to El Niño case (Figs. 1, 2b). This warming peaks in winter and spring, and can last till early summer, two seasons after the peak of ENSO, possibly maintained by local air–sea interactions over the Indian Ocean (Xie et al. 2009; Du et al. 2009). In addition to this basin-wide warming associated with ENSO, the Indian Ocean is also home to intrinsic SST interannual variability. A positive Indian Ocean Dipole (IOD) is characterized by strong negative SSTA near the coast of Sumatra and weaker positive SSTA in the western Indian Ocean (e.g. Reverdin et al. 1986; Saji et al. 1999; Webster et al. 1999; Murtugudde et al. 2000; Fig. 2a). Similar feedbacks to that occurring for ENSO in the Pacific allow the IOD to grow during summer in the

Fig. 2 Main SSTA patterns described in literature as likely to influence ENSO through atmospheric teleconnections: **a** the tropical Indian Ocean in fall, the southern Indian, Pacific and Atlantic Oceans in winter, the North Pacific in spring and the tropical Atlantic in summer; **b** the tropical Indian and the North Atlantic Oceans in spring. The patterns on these figures are obtained as the first EOF of the SST anomalies in each region at the targeted season



Indian Ocean and peak in boreal fall (Saji et al. 1999; Cai and Qiu 2013).

Previous studies had already proposed that signals in the Indian Ocean could be precursors of ENSO variability in the Pacific (e.g. Meehl et al. 2003; Clarke and Van Gorder 2003). Izumo et al. (2010) has further proposed that the cold SSTA in the IOD eastern pole drives a westerly wind anomaly over the tropical Pacific (Annamalai et al. 2010) that abruptly disappears in winter alongside with the rapid collapse of the IOD eastern pole. The oceanic response to this abrupt wind change induces a negative SSTA in the central Pacific in spring, which can be further amplified by the Bjerknes feedback to culminate into a La Niña at the end of the year. In contrast, other authors propose that it is the uniform basin-wide warming of the Indian Ocean associated with El Niño that produces an easterly wind anomaly over the western Pacific in winter (Annamalai et al. 2005), which favours the phase transition to La Niña (e.g., Kug and Kang 2006; Ohba and Ueda 2007). Jansen et al. (2009) and Frauen and Dommenges (2012) suggested that this Indian Ocean basin-wide variability indeed influences the ENSO cycle, but with no large impact on its predictability.

The two major modes of interannual variability in the Atlantic Ocean may also influence ENSO development. The first mode is known as “Atlantic Niño” (Zebiak 1993). “Atlantic Niños” peak in May–July and involve fluctuations of the equatorial Atlantic cold tongue (see the pattern in Fig. 2a) that are amplified by similar coupled air–sea feedback to those involved in ENSO and IOD development.

Some studies (e.g. Rodríguez-Fonseca et al. 2009; Losada et al. 2010; Martin-Rey et al. 2012; Ding et al. 2012) suggest that these “Atlantic Niños” may reinforce the ascending branch of the Walker circulation above the Atlantic and induce anomalous subsidence and surface easterly winds over the central Pacific, favouring a La Niña development. The studies of Jansen et al. (2009) and Frauen and Dommenges (2012) find a weaker influence of the equatorial Atlantic than of the Indian Ocean basin-wide variability on the ENSO cycle, but a larger influence of equatorial Atlantic Ocean initial conditions on ENSO forecasts. The second mode of tropical Atlantic SST variability is a meridional dipole pattern that peaks in boreal spring (Fig. 2b). Its warm (cold) pole is associated with relaxed (intensified) trade winds (Nobre and Shukla 1996), suggesting a development through wind–evaporation positive feedback (Chang et al. 1997). Ham et al. (2013) suggest that these warm SSTAs in the northern tropical Atlantic (0°–15°N) in boreal spring induce an anomalous cyclonic flow over the eastern Pacific. This leads to the development of easterly winds over the western equatorial Pacific through local air–sea interactions during the following summer, favouring a La Niña development.

Finally, Vimont et al. (2001, 2003) emphasize the potential influence of North Pacific mid-latitudes SST variability on ENSO (see the pattern in Fig. 2a) through the “footprinting mechanism”. In this mechanism, mid-latitude Pacific stochastic atmospheric fluctuations drive SSTAs in winter through latent heat fluxes (see e.g.,

Chiang and Vimont 2004). A feedback between trade winds and the meridional SST gradient favours the propagation of these SSTAs into the equatorial Pacific by the following boreal summer (Vimont et al. 2003). This SSTA in turn drives equatorial zonal wind anomalies, which influence ENSO development (Alexander and Vimont 2010). A similar influence of Southern hemisphere subtropical Pacific SSTA (see the patterns in Fig. 2a) has also been proposed (Terray 2010; Zhang et al. 2014; Boschat et al. 2013).

Most of the aforementioned studies focused on the influence of a particular region on ENSO. The studies of Jansen et al. (2009) and Frauen and Dommenges (2012) were the first one to compare the influence of two regions, finding a larger influence of the Indian Ocean on the ENSO cycle, but a larger impact of equatorial Atlantic initial conditions on ENSO forecasts. Dayan et al. (2013) is however to our knowledge the first study to adopt a systematic statistical approach in order to evaluate the respective influences of all the aforementioned regions on ENSO. They do so by identifying SST patterns outside the tropical Pacific that bring additional ENSO predictability to the one intrinsic to tropical Pacific. They identify the Atlantic meridional mode and South Pacific subtropical dipole mode in spring as well as the Indian Ocean Dipole and south Atlantic subtropical dipole mode as possible precursors of ENSO. The sensitivity of their results to the datasets and methodological approach however illustrates the difficulty to robustly identify regions that influence ENSO using a statistical approach based on available observations. These caveats motivate the development of a more dynamical approach in the present study. We will use an Atmospheric General Circulation Model (hereafter, AGCM) in order to investigate the equatorial wind response over the Pacific Ocean to forcing by SSTA in various regions. A simple ocean model will then be used to translate this remotely-forced equatorial Pacific wind response in terms of SST response.

In Sect. 2, we describe and briefly validate the AGCM and simple ocean model that we will use in this paper. In Sect. 3, we show that interannual wind anomalies still occur in the western Pacific in an AGCM ensemble in absence of interannual SST forcing over the tropical Pacific, illustrating that SST variations in the rest of the world can indeed

drive equatorial Pacific wind anomalies. In Sect. 4, we analyse AGCM ensembles with SSTA applied separately in the tropical Indian Ocean, subtropical North and South Pacific and tropical and North Atlantic ocean. In Sect. 5, we summarize and discuss our results.

2 The modelling strategy

2.1 The atmospheric general circulation model

ECHAM5 (Roeckner et al. 2003, 2004), developed at the Max Planck institute for Meteorology, is the fifth generation of the ECHAM AGCM, derived from the European Center for Medium-Range Weather Forecasts Integrated Forecasting System (Simmons et al. 1989). The version used in the current study is ECHAM 5.4 with a T106 (1.125°) horizontal resolution and 31 hybrid sigma-pressure levels. The Fouquart and Bonnel (1980) scheme is used for vertical shortwave transfer, while longwave transfer uses the “rapid Radiative Transfer Model” developed by Mlawer et al. (1997). A mass flux scheme is employed for shallow, mid-level and deep convection (Tiedtke 1989) with modifications for deep convection according to Nordeng (1994). The stratiform cloud scheme consists of prognostic equations for the water phases (vapor, liquid, solid), bulk cloud microphysics (Lohmann and Roeckner 1996), and a statistical cloud cover scheme with prognostic equations for the distribution moments (Tompkins 2002). The surface temperature over land is obtained from the surface energy balance (Schulz et al. 2001).

An Atmospheric Model Intercomparison Project-type control experiment was run with this configuration. This experiment is forced with the National Oceanic and Atmospheric Administration (NOAA) daily SST analysis (Reynolds et al. 2007) and sea ice data are taken from the NASA Goddard Space Flight Center (Cavalieri et al. 1999). A single member of this control experiment was run over a 29-years period from 1982 to 2010 (Table 1).

For our study, it is very important that the AGCM we use is able to reproduce atmospheric teleconnections. Figure 3 allows validating the global teleconnection pattern associated with ENSO, by regressing seasonal precipitation and wind stress data on the SST anomalies averaged

Table 1 Main characteristics of the CTL, CLIM and PACLIM AGCM experiments

Experiment	CTL	CLIM	PACLIM
SST forcing	Observed SST everywhere	SST climatology everywhere	SST climatology in 150°E–70°W; 15°S–15°N and interannual SST elsewhere
Time period	1982–2010	21 years	1982–2010
Members	1	1	7

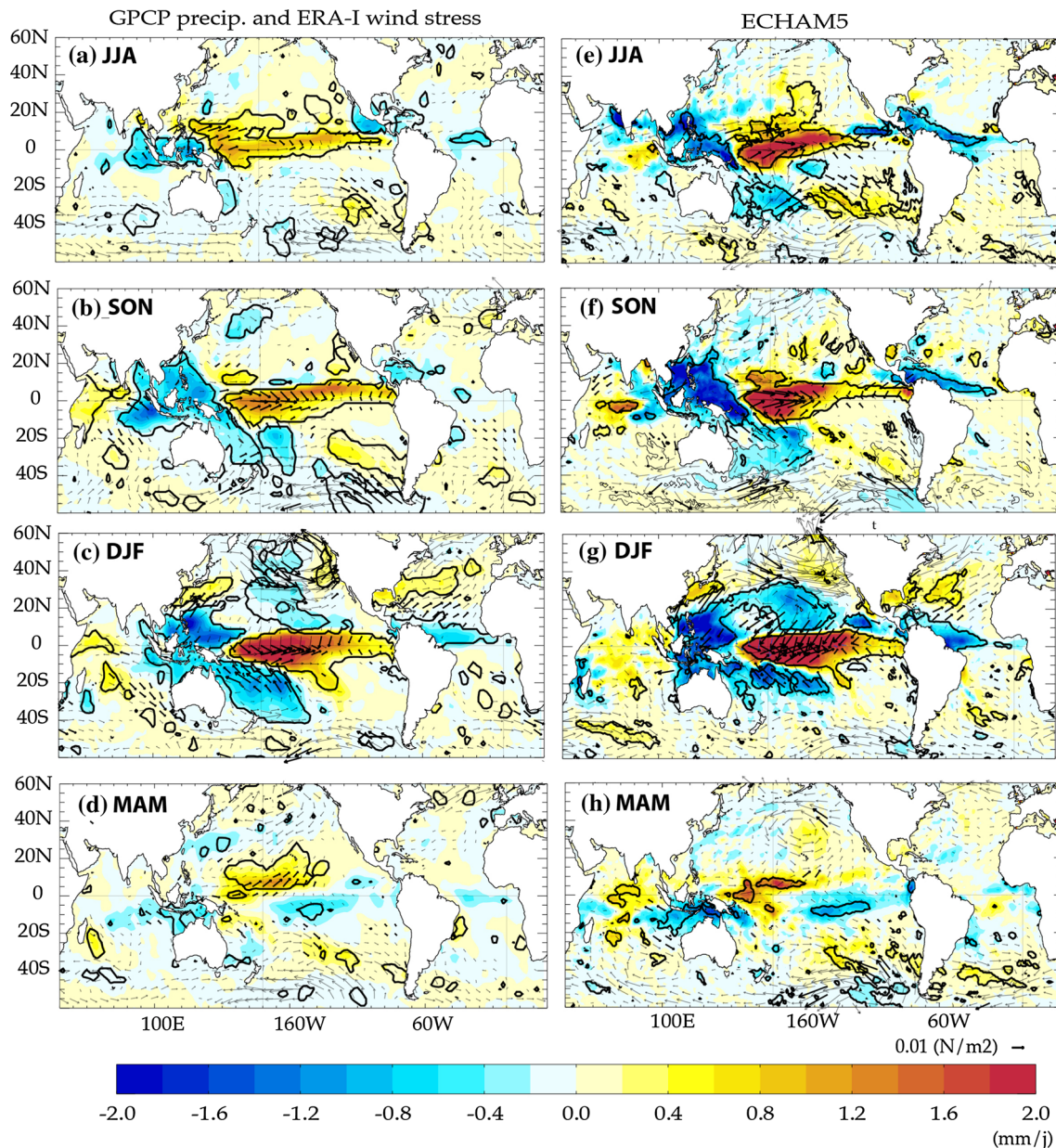


Fig. 3 ENSO global teleconnection patterns, illustrated from the regression between global seasonal (JJA, SON, DJF and MAM) precipitation and wind stress anomalies onto the Niño3.4 index, over the 1982–2009 period in **a** observations (ERA-I wind stresses and GPCP

precipitations) and **b** the CTL ECHAM5.4 experiment, forced by observed SST. Only regression coefficients that are significantly different from zero at the 95 % confidence level are plotted

in the Niño3.4 index (i.e. average SST anomalies in the 170°W – 120°W ; 5°S – 5°N box). The modelled ENSO teleconnection pattern is computed using CTL experiment output while the observed pattern is obtained from ERA-Interim (ERA-I; Dee et al. 2011) wind stresses and Global Precipitation Climatology Project (GPCP) Version 2.2 data (Adler et al. 2003). During observed El Niño events, tropical regions display reduced rainfall over the Indo-Pacific warm pool, the South Pacific Convergence Zone and the Atlantic Ocean Inter Tropical Convergence Zone

and increased rainfall in the western Indian Ocean and the central Pacific where strong westerly wind anomalies are evident. ECHAM5.4 generally reproduces these contrasted tropical patterns, with a tendency to overestimate their amplitude. The model also reproduces the tendency of weaker rainfall during El Niños within the Atlantic Ocean Inter Tropical Convergence Zone (ITCZ). By contrast, while the model also reproduces qualitatively well the IOD wind and rainfall anomalies in boreal fall, they are less intense and statistically significant than in

observations. The reasons for this bias are unclear (possibly too strong intraseasonal noise and/or systematic mean biases). Such biases will be kept in mind when discussing the results of the present study. Outside the tropics, the model accurately captures the remote surface wind response to ENSO: e.g. an anomalous cyclonic flow associated with the PNA over the northern Pacific in winter (e.g. Wallace and Gutzler 1981; Horel and Wallace 1981), and anomalous easterlies in the south-eastern Pacific Ocean most clearly in DJF.

As we aim at investigating teleconnections between SST forcing outside of the tropical Pacific and wind stress in the equatorial Pacific, we also assess the model ability to simulate wind stress variations in the western Pacific. The average monthly ZWSA within the 125°E–160°W; 3°S–3°N box (the choice of this box will be justified later in this paper) in CTL has a relatively high 0.64 correlation with ERA-I (given the fact that CTL also includes random intraseasonal variability uncorrelated with the observed one).

2.2 The simple ocean model

The dynamical response of the equatorial Pacific upper ocean to zonal wind stress can be in good approximation estimated from a linear shallow water model (e.g. McCreary 1976; Federov and Brown 2009). Linear shallow water equations have in particular been used to study ENSO-like variability in the oceanic component of several coupled models (e.g., Zebiak and Cane 1987). The tropical Pacific configuration in the current study has an idealised coastline, a mean upper layer mean depth of 100 m and a reduced gravity of 0.062 m s⁻², in order to produce a realistic equatorial Kelvin wave phase speed of 2.5 m s⁻¹ (see Izumo et al. 2010 for more details).

The shallow water model produces a solution in terms of depth of the upper layer (a proxy for the thermocline depth) and upper layer currents anomalies. We use a simple method to estimate equatorial Pacific SSTA from those. SST variability is driven by three main processes: lateral advection, heat fluxes at the air–sea interface, and exchange between the mixed layer and subsurface (either as the result of upwelling, vertical mixing or entrainment, e.g. Niiler and Kraus 1977). Several studies have shown that zonal advection plays a strong role in driving SSTA in the central Pacific at interannual time scales (e.g. Picaut et al. 1996), while vertical processes are more dominant in the eastern Pacific: the deepening of the thermocline decreases the surface cooling, due to upwelling and vertical turbulence (e.g. Vialard et al. 2001). In general, air–sea fluxes tend to damp the growth of SSTA and can usually be represented as a Newtonian damping of the SST anomaly (e.g., Wang and McPhaden 2000; Vialard et al. 2001). We thus use a

very simple equation to obtain the SSTA T' in the equatorial band from the upper layer zonal currents U' and thermocline depth anomalies H' :

$$\frac{\partial T'}{\partial t} = -U' * \frac{\partial \langle T \rangle}{\partial x} + \alpha * (\gamma * H' - T') \quad (1)$$

The first term of the right hand side represents the zonal advection of the mean temperature $\langle T \rangle$ zonal gradient by interannual anomalies of the surface current U' . The climatological temperature $\langle T \rangle$ is obtained from the TRMM Microwave Imager (TMI) SST (Wentz et al. 2000) 1998–2007 average. The surface heat flux negative feedback on the SST anomalies is represented by the Newtonian relaxation $-\alpha T'$. The tendency of a thermocline anomaly H' to favour or inhibit cooling by vertical processes is represented as $\alpha \gamma H'$. We use this simple parameterization with $\alpha = 0.36 \text{ month}^{-1}$, and with a $\gamma = 0.0077 \text{ km}^{-1}$ γ value east of 140°W, which linearly decreases to one fifth of this value at the western boundary in order to mimic the decrease of upwelling cooling strength towards the west. The α and γ values were derived from observations by Burgers (2005) for the central-eastern Pacific; and we use the same longitudinal dependency of as McGregor et al. (2009).

Whereas the above equation does not allow accurately simulating SSTA in the western Pacific, it is appropriate for the central-eastern Pacific, which is the key region for the Bjerknes feedback. In order to validate this simple approach to estimate SSTA, we performed a control integration of the shallow water model, forced by ERA-I wind stresses over the 1979–2009 period, starting from rest. Despite the simplicity of our approach, the shallow water model and simple SST equation (1) perform surprisingly well at reproducing SSTA in Niño3.4 (Fig. 4), with a correlation coefficient of 0.8 and rms-difference of 0.46 °C with observed SSTA.

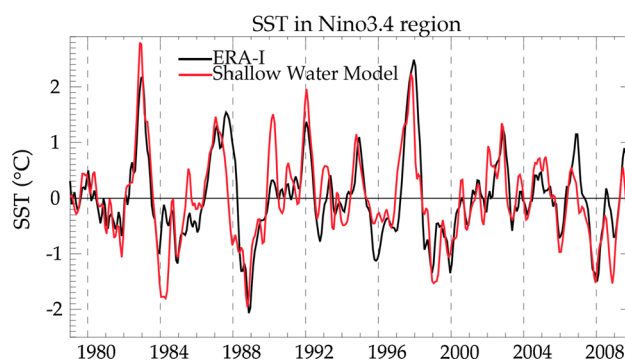


Fig. 4 Niño3.4 index (average SSTA in the 170°W–120°W; 5°S–5°N box) from ERA-I (black curve) compared to a control run of the simple ocean model (red curve) forced by the ERA-I tropical Pacific interannual wind stress anomalies from 1979 to 2009. These time series are correlated at 0.8 with a RMS-error of 0.46 °C

2.3 Experiments design

Two types of ensemble AGCM experiments have been performed for this paper: (1) long experiments (20 years or more) using either climatological or inter-annually varying SST in various regions; (2) shorter 2-years experiments with SST perturbations applied in various regions. We describe the long experiments in the current section. The shorter experiments are motivated by the results of Sect. 3 and will be described at the beginning of Sect. 4.

The long experiments used in the present study are summarized in Table 1. The control experiment (CTL) has been described in Sect. 2.1: it is run over 1982–2010 and forced by observed interannually varying SST and sea-ice cover. Two additional experiments using the 1982–2010 mean SST and sea-ice cover seasonal cycle have been performed. The CLIM experiment is forced by a smooth mean seasonal cycle. A single member of this experiment was run over a 21 years period, and only the 20 last years of that experiment are considered in this paper. The PACLIM experiment allows assessing if SST variability outside the tropical Pacific can remotely drive inter-annual wind anomalies in the equatorial Pacific. This experiment is run over a 29-years period (1982–2010), forced by the same mean seasonal cycle of SST as CLIM over the tropical Pacific and interannual forcing elsewhere. The SST climatology is applied within the 165°E–75°W;15°S–15°N domain, and a smooth linear transition to observed SST is applied over a ~10° buffer zone (see Fig. 5a). This experiment consists of seven ensemble members. The ensemble was constructed by applying small perturbations (spatial white noise of 0.01 °C amplitude) to the SST forcing during the first day of the AGCM experiment. If one assumes that after a few weeks, the internal variability is fully independent in each member, the contribution of atmospheric noise to the model response should be divided by about 2.6 ($\sqrt{7}$).

Oceanic experiments using the shallow water model described in Sect. 2.2 and forced by wind stress anomalies from each of the ensemble member of the experiments above have been performed in order to evaluate the tropical Pacific Ocean response to remotely-forced equatorial Pacific wind stress anomalies.

3 Is there an externally-forced wind signal over the Pacific?

The PACLIM experiment uses a climatological seasonal cycle of tropical Pacific SST, but observed SST during the 1982–2010 period in other regions. Interannual wind stress anomalies in the tropical Pacific in this experiment can thus only be the result of residual stochastic variability in

the atmosphere or of remote forcing from SSTA in other regions.

Figure 5b shows the standard deviation of equatorial zonal wind stress interannual anomalies in the CTL and the ensemble mean of PACLIM experiments. The CTL experiment overestimates the zonal wind stress interannual variability in the equatorial Pacific. We will come back to this point in the discussion section. The use of climatological SST in the tropical Pacific of course strongly reduces the amplitude of wind stress anomalies, but significant wind stress inter-annual variations still persist, especially in the western Pacific (Fig. 5b), within the 125°E–160°W, 3°S–3°N box. Figure 6 shows the average zonal wind stress within this box, as well as the ensemble spread. The PACLIM western Pacific wind stress displays coherent variations lasting from a few months to almost 1 year. These anomalies, often significantly different from zero, are therefore not a residual from internal variability of the AGCM. This suggests a potential atmospheric teleconnection between some regions outside the tropical Pacific and the zonal wind stress variability in the western equatorial Pacific basin.

The shallow water model and simple equation (1) allow translating the Pacific wind stress variations of each PACLIM ensemble member into an estimated SSTA response. Figure 5c shows that this oceanic response is largest in the central Pacific (in the Niño3.4 box), with a standard deviation exceeding 0.4 °C. The Niño3.4 SSTA response to PACLIM winds can be seen in Fig. 6. This SSTA response regularly reaches a ~1 °C amplitude over the Niño3.4 box, over a few months to 1 year. Although this is less than the amplitude of ENSO itself, the results of our forced ocean experiment do not include the coupled Bjerknes feedback, which could amplify those SSTA.

Figure 7 shows the seasonal distribution of the amplitude of zonal wind stress fluctuations in the western Pacific box and of the corresponding SSTA response in the Niño3.4 region. The largest wind stress variations occur during boreal winter (December–March) in the PACLIM experiment. The ocean response is delayed by ~4 months and occurs in boreal spring (April–June). These analyses suggest that the strongest remotely-forced wind stress anomalies over the western Pacific probably occur in boreal winter, with the strongest response in the central Pacific in boreal spring, the season when the equatorial Pacific atmosphere is most sensitive to SSTA and favourable to ENSO onset (e.g. Spencer 2004).

The potential influence of these SST fluctuations on the ENSO cycle can be inferred by computing the lead-correlation between these SSTA and the Niño3.4 index during the following ENSO peak in NDJ (not shown). These SSTA display a weak (0.35) but statistically significant at the 95 % level, correlation with the next ENSO peak in April

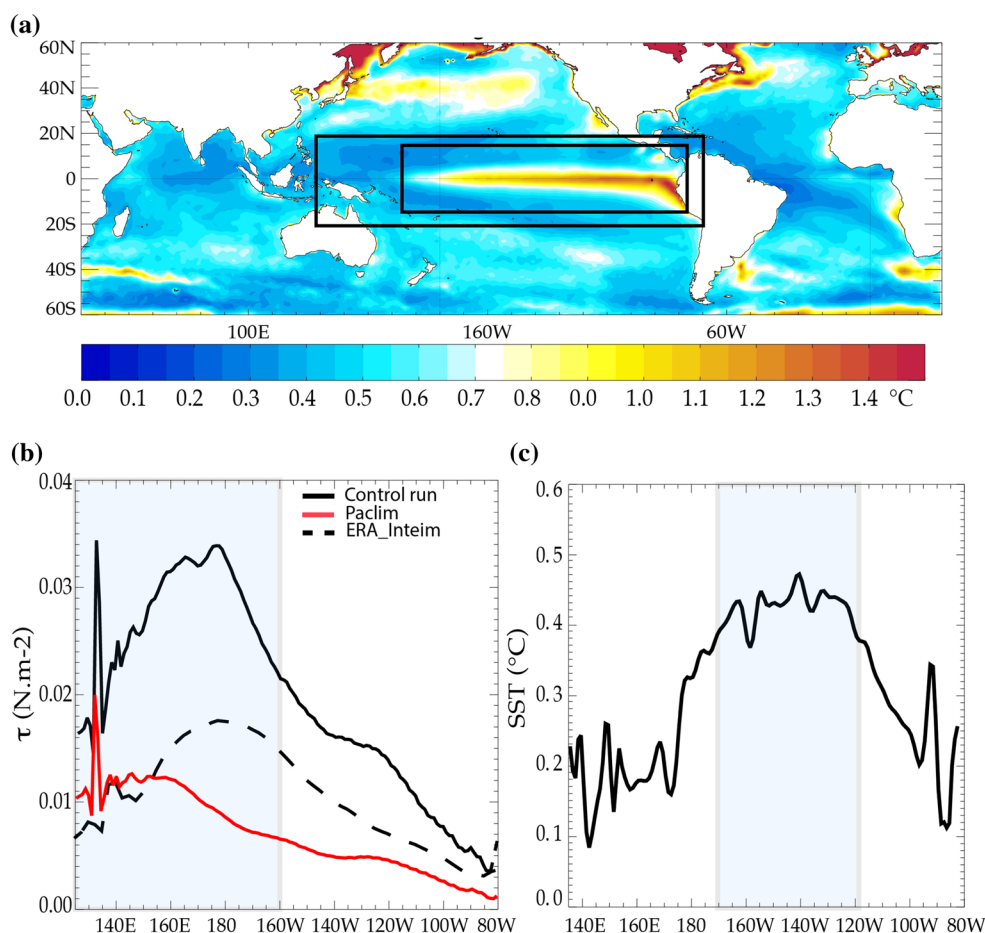


Fig. 5 **a** Standard deviation of the global SST interannual anomalies used to force the CTL ECHAM5.4 experiment. The *inner black box* (165°E–75°W; 15°S–15°N) indicates the region in which the PACLIM experiment is forced by climatological SST; the PACLIM experiment is forced by observed SST outside of the *outer black box*. A smooth transition between the SST climatology and full interannual SST is applied in the transition region. **b** Standard deviation of the equatorial (3°S–3°N) ZWSA in the CTL (*black curve*), the ensemble mean of PACLIM (*red curve*) experiments and in the ERA-I reanalysis (*dashed black curve*). The *shaded blue box* delin-

eates the western Pacific region (125°E–160°W; 3°S–3°N) where residual wind stresses forced by SSTA from outside the Pacific are the largest: the CTL run reproduces reasonably the observed zonal wind stress variability observed in this *box*, with a correlation of 0.64 with ERA-I wind stresses. **c** Standard deviation of the equatorial (5°S–5°N average) SST anomalies from the simple ocean model ensemble run in response to the PACLIM wind stress. The *shaded blue box* indicates the Niño3.4 box in which the SST response to PACLIM wind stresses is the largest

(i.e. when the SST response to the PACLIM ZWSA is largest). This weak correlation can be interpreted as the sign that SSTA in the central Pacific induced by remotely-forced wind stress variations could (weakly) favour ENSO onset.

These results suggest that regions outside the Pacific can induce wind stress variations in the tropical Pacific that can moderately interfere with the ENSO evolution. The exact region outside of the tropical Pacific controlling these wind variations however remains to be identified. Figure 8 displays the seasonal correlation between the global SST (used to force the PACLIM experiment) and the PACLIM ensemble-mean wind stresses in the western equatorial Pacific Ocean. Surprisingly, the patterns displayed on Fig. 8 are somehow reminiscent (with opposed polarity) to that

of Fig. 1, which shows the global teleconnection pattern of ENSO. This indicates that easterly wind anomalies tend to develop in the western Pacific in PACLIM during El Niño events. Since PACLIM does not use SST interannual forcing in the tropical Pacific, this suggests that these easterly anomalies may be the result of the El Niño teleconnection pattern. I.e. that ENSO influences the SST outside of the Pacific through atmospheric teleconnections, but that some of these SSTAs feedback negatively on ENSO. This scenario resembles the one proposed by some previous studies (e.g. Kug and Kang 2006; Ohba and Ueda 2007) for the influence of the Indian Ocean basin-wide warming on ENSO.

The analysis of Fig. 8 does not allow identifying which region (or regions) remotely forces the PACLIM ZWSA

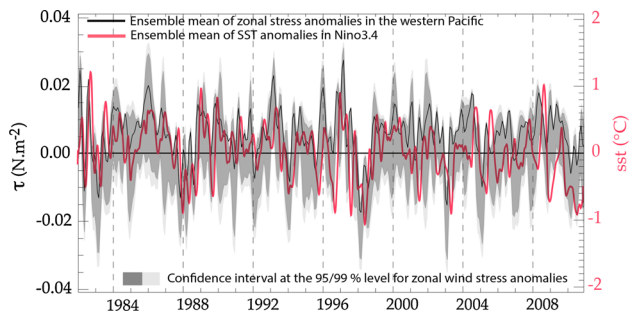


Fig. 6 Ensemble mean of PACLIM ZWSA (black curve) in the western equatorial Pacific box (125°E–160°W; 3°S–3°N) and of the resulting SST anomalies response in the Niño3.4 region (red curve) derived from the simple ocean model. The dark (light) grey shading indicates the 95 % (99 %) confidence interval for the ZWSA ensemble mean, computed from the spread of the seven members. The confidence interval for the SST anomalies is not shown on this figure for clarity

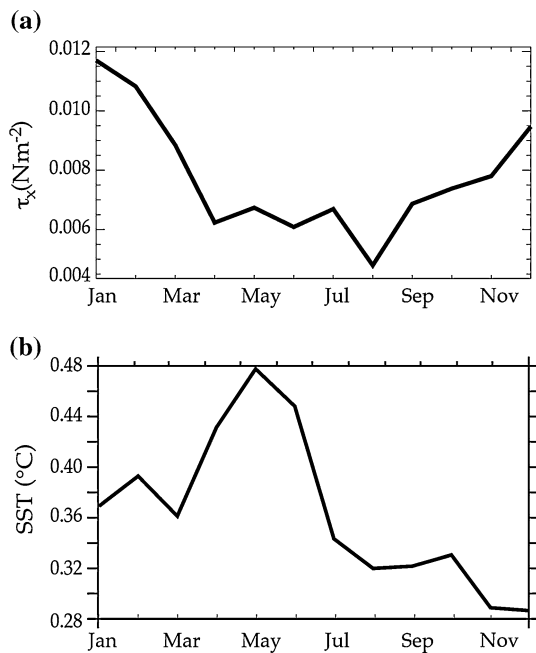


Fig. 7 Seasonal cycle of the standard deviation of **a** PACLIM equatorial ZWSA in the western equatorial Pacific box (125°E–160°W; 3°S–3°N) and **b** of the SST interannual anomalies in the Niño3.4 region of the simple ocean model forced by PACLIM wind stresses

in the western Pacific. In order to narrow-down the main forcing region, we have performed sensitivity experiments with idealised SST anomalies selectively applied in various regions in the following section. Figure 8 provides a good guidance for selecting these regions and the associated climate modes for each region. In the Indian Ocean, the pattern is reminiscent of the basin-wide warming associated with ENSO, clearest in DJF and MAM (compare Fig. 8c, d

and Fig. 2b), although an IOD-type structure is also visible in SON (compare Fig. 8b with Fig. 2a). In the mid-latitude Pacific Ocean, the pattern is most visible in DJF and MAM (Fig. 8c, d) and is very comparable with the ENSO teleconnection patterns (i.e. the PNA in the Northern Pacific and its southern Pacific counterpart, cf Fig. 2a, b). It is more difficult to clearly distinguish one of the main modes of variability of the Atlantic Ocean on Fig. 8, which displays features that are both reminiscent of the “Atlantic Niño” (Fig. 2a) and Atlantic meridional dipole (Fig. 2b) depending on the seasons. In general, however, Fig. 8 motivates to investigate the remote signatures over the equatorial Pacific of the following climate modes: the IOD and basin-wide warming for the Indian Ocean, the mid-latitude “footprints” of atmospheric variability for the Northern and Southern Pacific and the Atlantic Niño and meridional modes. In the following section, we will design sensitivity experiments that allow diagnosing the remote response of the Pacific Ocean to the SST patterns corresponding to each of those climate modes.

4 In which region do SST anomalies induce a response of the equatorial Pacific?

In this section, we first describe our strategy for constructing sensitivity experiments with selectively-applied SST perturbations in the Indian Ocean, North and South Pacific and Atlantic Ocean (Sect. 4.1). We then compare the equatorial Pacific wind stress and SSTA response to interannual SST forcing in those regions (Sect. 4.2): our analysis reveals that the only region that induces a statistically significant SSTA response in Niño3.4 is the Indian Ocean. We then focus on the teleconnection pattern and mechanisms of the Pacific response to the tropical Indian Ocean forcing in more details in Sect. 4.3.

4.1 Description of the sensitivity experiments

In order to identify regions in which SSTA are susceptible of inducing a wind stress response over the tropical Pacific, we ran several 1-year, 20-members ensemble experiments with climatological SST everywhere, except in targeted regions, where composite SSTA representative of a given regional climate mode were applied (see Table 2 for a summary of these experiments). The 20-members ensembles were constructed by using the initial states on January 1 from each of the 20 years of the CLIM experiment. The mean response of the atmosphere to each SSTA pattern is then obtained from the ensemble average of the difference between each 2-years sensitivity experiment and the CLIM experiment. The use of 20 members should reduce the contribution of atmospheric noise to the model response by about 4.5 ($\sqrt{20}$).

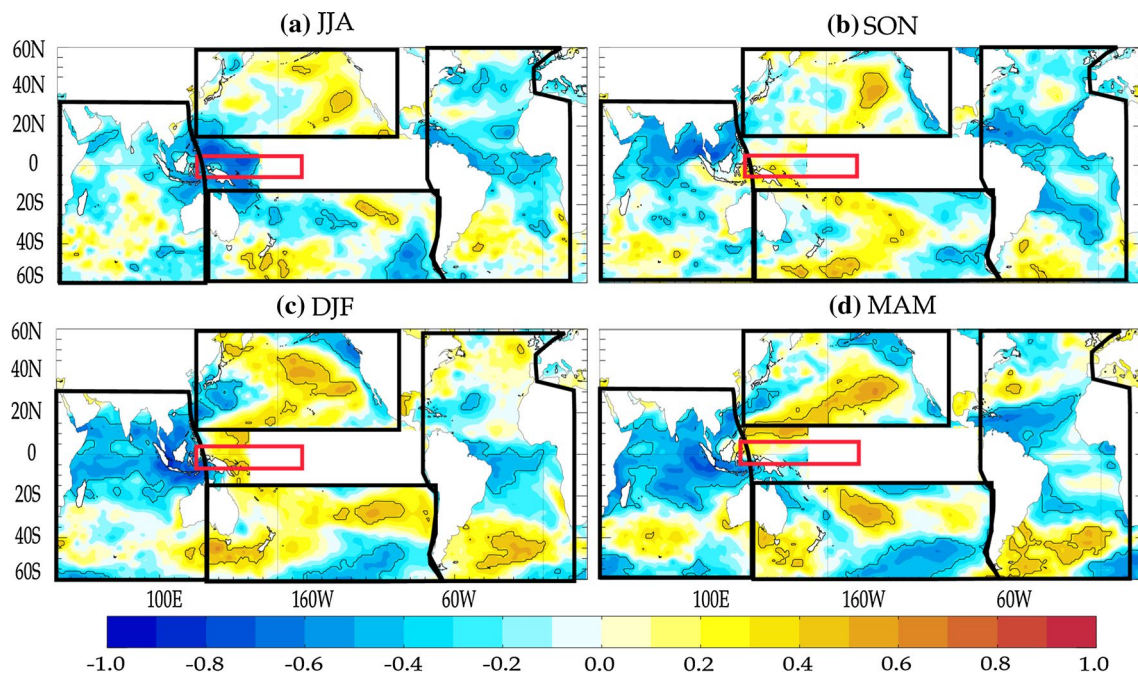


Fig. 8 Synchronous correlation between the PACLIM ZWSA in the western equatorial Pacific box (indicated by a red box on the plot) and the global SST interannual anomalies that were used to force the PACLIM experiment for **a** June–August, **b** September–November, **c** December–February and **d** March–May. The black boxes indicate the main regions in which the SST anomalies are correlated

with the PACLIM ZWSA. They allow defining the main sensitivity experiments of Table 2, meant to assess the influence of each of these regions separately on western equatorial Pacific wind stresses (see Fig. 9). Correlation coefficients that are significantly different from zero at the 95 % confidence level are indicated by the black contour

Table 2 Main characteristics of the IOD, IOB, NPAC, SPAC, ATL_NINO and ATL_MERID sensitivity experiments

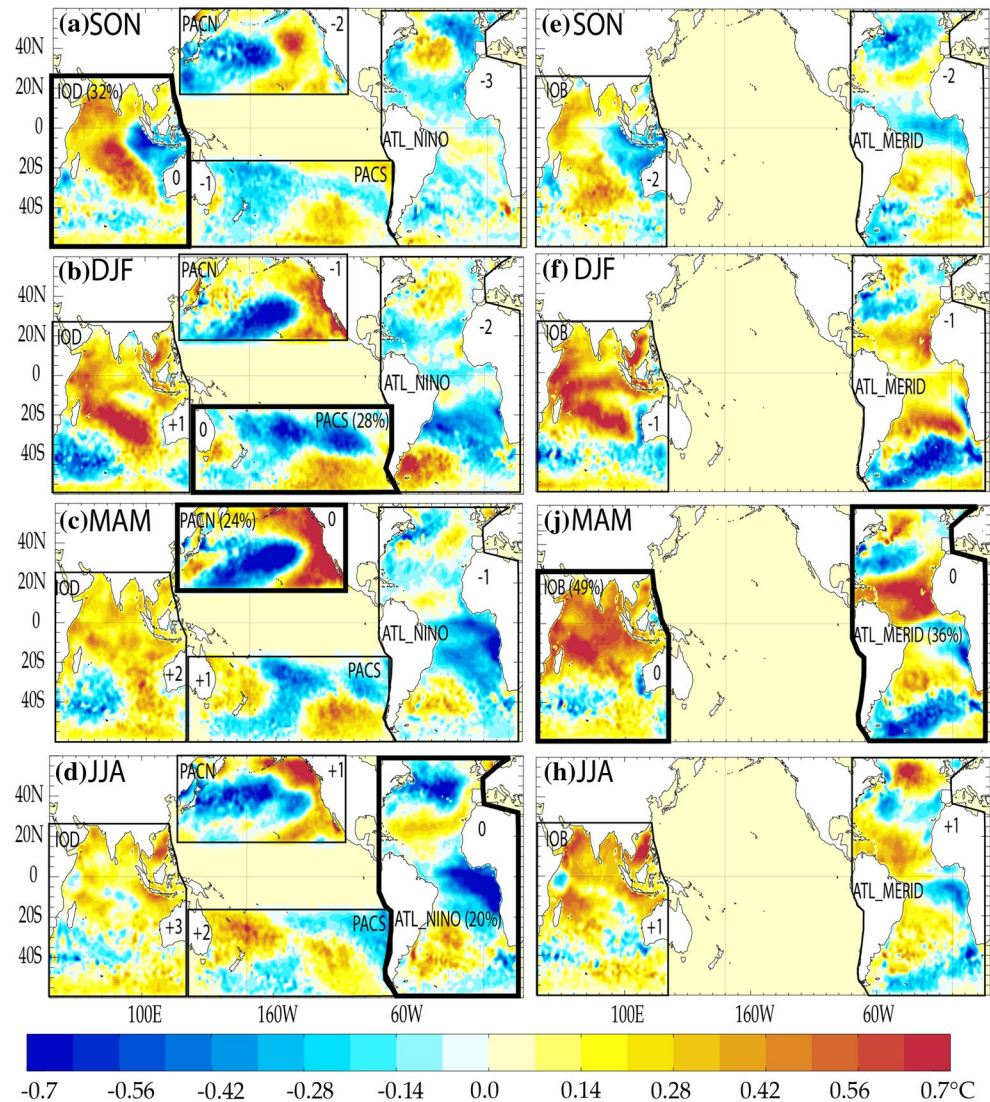
Experiment	IOD	IOB	NPAC	SPAC	ATL_NINO	ATL_MERID
SSTA applied in	30°E–130°E; 60°S–30°N	30°E–130°E; 60°S–30°N	120°E–110°W; 15°N–60°N	140°E–70°W; 60°S–15°S	70°W–20°E; 60°S–60°N	70°W–20°E; 60°S–60°N
EOF computation season (reference year)	SON (yr0)	MAM (yr1)	MAM (yr1)	DJF (yr0–1)	JJA (yr1)	MAM (yr1)
Members	20	20	20	20	20	20

Each of these experiments lasts 2 years (from January of year 0 to December of year 1) and has 20 ensemble members. The SST climatology is applied everywhere, with a SST anomaly only applied in a selected region. This SST anomaly is applied over the entire 2 years, but computed from the EOF analysis of SST in the specific region at a selected season (see text for details and Fig. 9 for the SSTA anomalies applied in each region)

As explained at the end of Sect. 3, the analysis of the PACLIM experiment suggests that the SST patterns of several climate modes may influence winds in the equatorial Pacific: the IOD and IOB in the Indian Ocean, mid-latitude footprints of atmospheric variability in the North (NPAC) and South (SPAC) Pacific and the Atlantic Niño (ATL_NINO) and meridional mode (ATL_MERID). Here, we briefly describe how SSTA composites representative of these modes of variability were obtained to perform the sensitivity experiments (see Table 2 for a definition and Fig. 8 for the boundary of these regions). To define the 1-year-long daily inter-annual SST anomalies applied in

each region of interest, we first computed the first EOFs of the covariance matrix of the large-scale inter-annual SST anomalies in this region, at the season indicated in Table 2. This season was selected for each region based on a literature review of the main teleconnection between SST in this region and the Pacific: the IOD peak (SON; Izumo et al. 2010) and the IOB in MAM (e.g. Ohba and Ueda 2007; Xie et al. 2009) for the Indian Ocean; spring for the Northern Pacific (Vimont et al. 2001); winter for the Southern Pacific (Terray 2010); spring for the Atlantic meridional mode (Ham et al. 2013) and summer for the Atlantic Niño (Rodríguez-Fonseca et al. 2009). The daily composite SSTA

Fig. 9 SSTA applied in the IOD, PACN, PACS, and ATL_NINO (*left panels*) and IOB and ATL_MERID (*right panels*) sensitivity experiments. The SSTA are displayed on the same map for presentation purposes, but are applied separately in a dedicated experiment for each region. They were obtained as twice the lead-lag regression onto the normalised principal component of the first EOF of SSTA at the season *outlined by a bold frame* (the % of variance explained by this EOF at that season is indicated). Each experiment lasts 2 years, from January (yr0) to December (yr1; see Table 2 for more details on their definition)



patterns were then obtained by a lead-lag regression of the daily SSTA in each region to its EOF principal component. In order to emphasize the response to rather large events rather than casual ones, the SSTA anomalies applied in each experiment (and displayed on Fig. 9) was multiplied by two, in order to represent rather large events (two standard deviations). Each sensitivity experiment begins in January and lasts 2 years to prevent side effects due to the data filtering. Only seasons suggested in the literature as being a window of opportunity for influencing winds in the Pacific are analysed in this paper (SSTA forcing for each region from SON(year0) to JJA(year + 1) is shown in Fig. 9).

In the Indian Ocean, for the IOD sensitivity experiment, the SSTA forcing pattern clearly captures the IOD SSTA dipole pattern in SON, and the following basin-wide warming in DJF and MAM (e.g. Xie et al. 2009). In the IOB sensitivity experiment, the SST pattern is qualitatively similar to the SSTA forcing in the IOD experiment, although with

warmer SSTA during the basin-wide warming in DJF and MAM and a weaker IOD in SON. I.e. the IOD and IOB experiments both include the successive IOD and IOB patterns, but each with a slightly larger amplitude at their peak season. The amplitude of these SSTA patterns applied in the Indian Ocean are of the same order of magnitude than the positive IOD event of SON 1997 and the following IOB in spring 1998. In the North and South Pacific, the resulting SST pattern in boreal winter and spring is clearly reminiscent of the “horseshoe” response to ENSO seen in Fig. 1, and of the mid-latitude stochastically-driven large scale SSTAs, or “footprints”, in these regions (e.g., Frankignoul and Hasselmann 1977; Trenberth et al. 1998; Deser and Wallace 2003; Deser et al. 2010). The SST pattern in the Atlantic in boreal spring (summer) is reminiscent of the northern (eastern equatorial) pole of the Atlantic Meridional Mode (Atlantic Niños). There are many possible choices for constructing SSTA patterns that are typical of the dominant

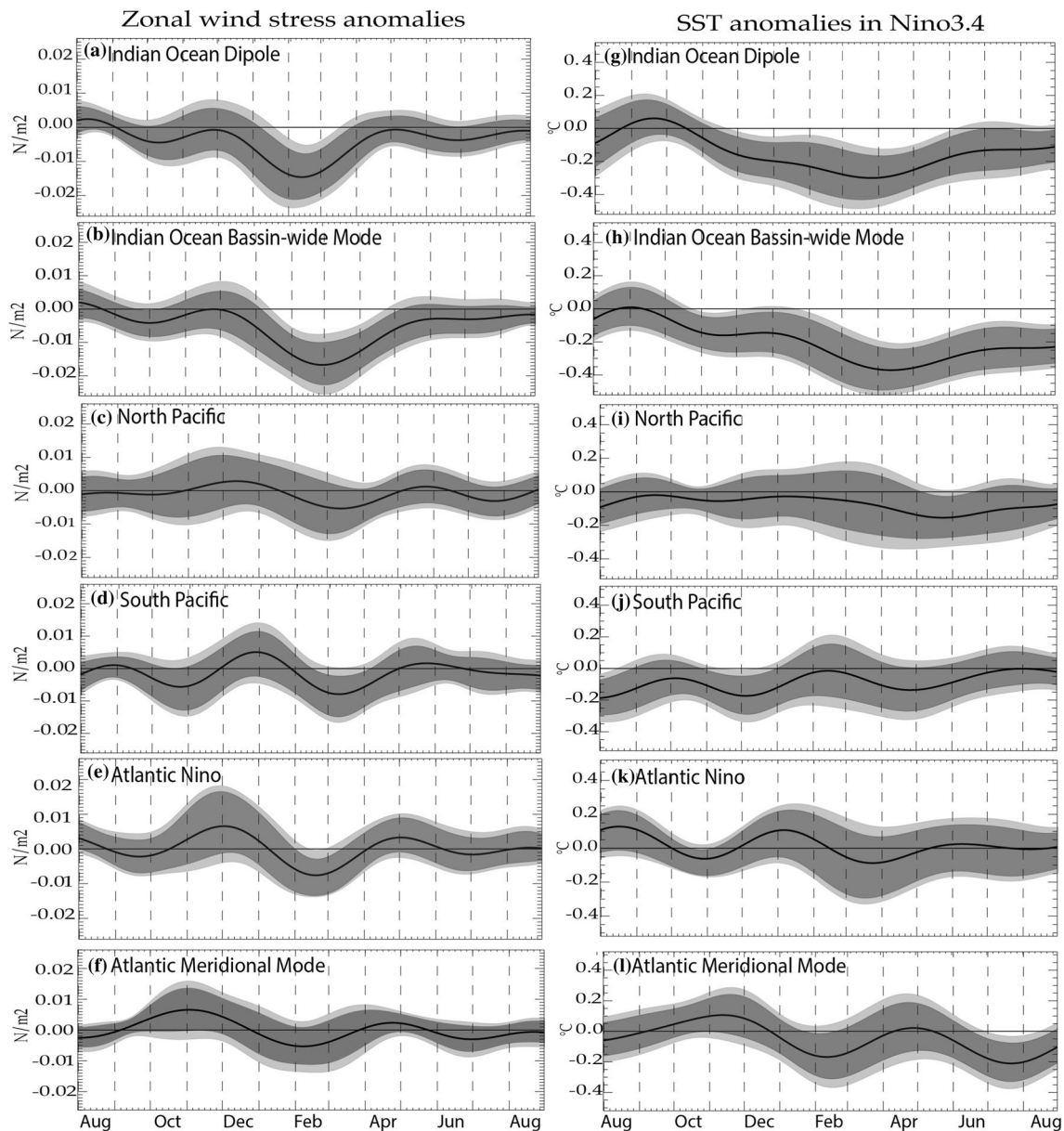


Fig. 10 The *left panels* show the ensemble mean of (*left*) the ZWSA in the western Pacific box (box shown on Fig. 9) and (*right*) the model SSTA response to these wind anomalies in the Niño3.4 region for the **a** IOD, **b** IOB, **c** NPAC, **d** SPAC, **e** ATL_NINO and

f ATL_MERID experiments. The 95 % (*dark grey shading*) and the 99 % (*light grey shading*) confidence intervals are based on a Student's *t* test, computed from the inter-member standard deviation in the 20-members ensembles

climate modes in each region, and we will discuss in Sect. 5.2 the possible consequences of the choices taken here.

4.2 Pacific Ocean response to SSTAs in the four selected regions

In this section, we seek to identify regions where SST inter-annual anomalies can significantly influence equatorial Pacific zonal wind stresses and produce a sizable SSTA in the central Pacific, that could ultimately be amplified by

the Bjerknes feedback and contribute to the ENSO cycle. Left panels of Fig. 10 exhibit the time evolution of ZWSA ensemble mean in the $125^{\circ}\text{E}\text{--}160^{\circ}\text{W}$; $3^{\circ}\text{S}\text{--}3^{\circ}\text{N}$ box, relative to the climatology provided by the CLIM experiment. All experiments display relatively small Pacific ZWSA perturbations (around 0.01 N m^{-2} in absolute value) compared to typical anomalies associated to ENSO (standard deviation of $\sim 0.03\text{ N m}^{-2}$ in the box defined above). The grey (light) shading on Fig. 10 indicates the 95 % (99 %) level confidence interval associated with different realizations of

internal atmospheric variability amongst ensemble members. The IOD and IOB experiments tend to produce larger wind anomalies than the other experiments. As a result, only these IOD and IOB experiments produce statistically significant ZWSA in the western equatorial Pacific at the 99 % level confidence interval in winter and early spring. In the other sensitivity experiments (PACS, PACN, ATL_MERID and ATL_NINO), the ensemble-average ZWSA over the equatorial western Pacific is smaller, never exceeding 0.005 N m^{-2} in absolute value, and is not significantly different from zero at the 99 % level (and only rarely at the 95 % level). Although the wind response in IOD and IOB experiments is qualitatively similar, the IOB wind response is slightly stronger (maximum of -0.02 N m^{-2} as compared to -0.015 N m^{-2} ; Fig. 10a) and lasts longer (until end of May as compared to mid-April) than the IOD wind response. In any case, these results suggest that, amongst the four tested regions, only Indian Ocean SSTA can induce a sizable zonal wind stress response over the equatorial Pacific. We will discuss this further in Sect. 5.2.

The right panels in Fig. 10 show the ensemble mean SSTA response to the ZWSA in the Niño3.4 region. As could be expected, the only experiments that produce a statistically significant SSTA response in the Niño3.4 region at the 99 % level confidence interval are the IOB and IOD experiments. The largest SST anomalies occur in March–May in both cases, about one month after the largest forcing in February–March. As a consequence of the stronger and more persistent wind forcing resulting from the IOB experiment, the resulting SSTA response is also slightly larger ($0.35 \text{ }^\circ\text{C}$ against $0.3 \text{ }^\circ\text{C}$) and lasts longer (until end of August against the end of May) compared to the IOD experiment. This SSTA response is quite small but corresponds to $\sim 35 \%$ of observed standard deviation at that season. In the following section, we discuss the teleconnection pattern that gives rise to the wind stress anomaly over the Pacific Ocean, and the mechanisms of the SSTA response.

4.3 Pacific atmospheric and oceanic response to Indian Ocean forcing

Figure 11d–f and g–i illustrates the seasonal atmospheric response to the IOD/IOB SSTA sequences shown in Fig. 9. A Student *t* test was performed to highlight regions whose wind stress response to SSTA in these experiments is significantly different from the CLIM experiment (which is forced by climatological SST everywhere). The wind stress and rainfall patterns of the IOD/IOB experiments are very similar, which is not surprising given the similarity of the two SST forcings (Fig. 9). Both experiments hence describe successively the atmospheric response to the IOD and then to the IOB SSTA patterns, with slightly more amplitude during SON for the IOD experiment and DJF–MAM for the

IOB experiment. We will thus discuss the results of these two experiments collectively.

The simulated atmospheric circulations in response to IOD/IOB SSTA patterns can be compared with Fig. 11a–c, which displays the precipitation and wind stress patterns obtained by regressing GPCP estimates and the ERA-I re-analysis to the IOB index (rather similar patterns are obtained when regressing on the IOD index, not shown). The observational counterpart in panels a–c of course contains both the remotely-forced response from ENSO and the response to local SST anomalies in the Indian Ocean, but it can at least be compared to the model response in the regions that are most directly affected by the IOD/IOB. In the equatorial Indian Ocean, the modelled response is qualitatively similar to the observational analysis in SON, with a clear IOD pattern (easterly wind anomalies and a precipitation dipole between the east and west Indian Ocean). This signal somewhat lingers on in DJF. The agreement is more qualitative in MAM, but both sensitivity experiments display negative precipitation/northeasterly wind anomalies in the Northern hemisphere and anomalies of opposite polarities in the Southern hemisphere, as ERA-I/GPCP, i.e. the asymmetric mode of tropical Indian Ocean rainfall variability in boreal spring discussed by Wu et al. (2008). The overall agreement between the model response to the IOD/IOB and Fig. 11a–c suggests that our ECHAM-5 simulation responds reasonably to SST anomalies in the Indian Ocean, a prerequisite for our experiments to be meaningful.

Let us now describe the processes of the atmospheric response in more details. During SON, both the IOD and IOB experiments exhibit a positive IOD signature in the Indian Ocean, with a statistically significant negative precipitation anomaly in the eastern tropical Indian Ocean (Fig. 11). This atmospheric response mainly results from decreased deep atmospheric convection induced by the SST cooling along the coasts of Java and Sumatra, typical of IOD events. Statistically significant easterly anomalies develop during SON in the eastern Indian Ocean in association with suppressed convection, as expected from the Gill model (Gill 1980). Statistically significant positive precipitation anomaly (i.e., increased deep convection) appears in the southwestern part of the basin, probably driven by warm SSTA there. SSTA anomalies in the Indian Ocean however does not force any significant wind anomalies over the equatorial Pacific during that season. During the following boreal winter and spring, the IOD cold eastern pole disappears, and the southern tropical Indian Ocean warms up (Fig. 9, e.g. Xie et al. 2009), resulting in a statistically significant positive precipitation anomaly in this region. In response to this basin-scale tropospheric warming, statistically significant westerly anomalies develop in the southwestern tropical Indian Ocean, west of the heat source (in DJF, Fig. 11), as expected from the Gill (1980) model.

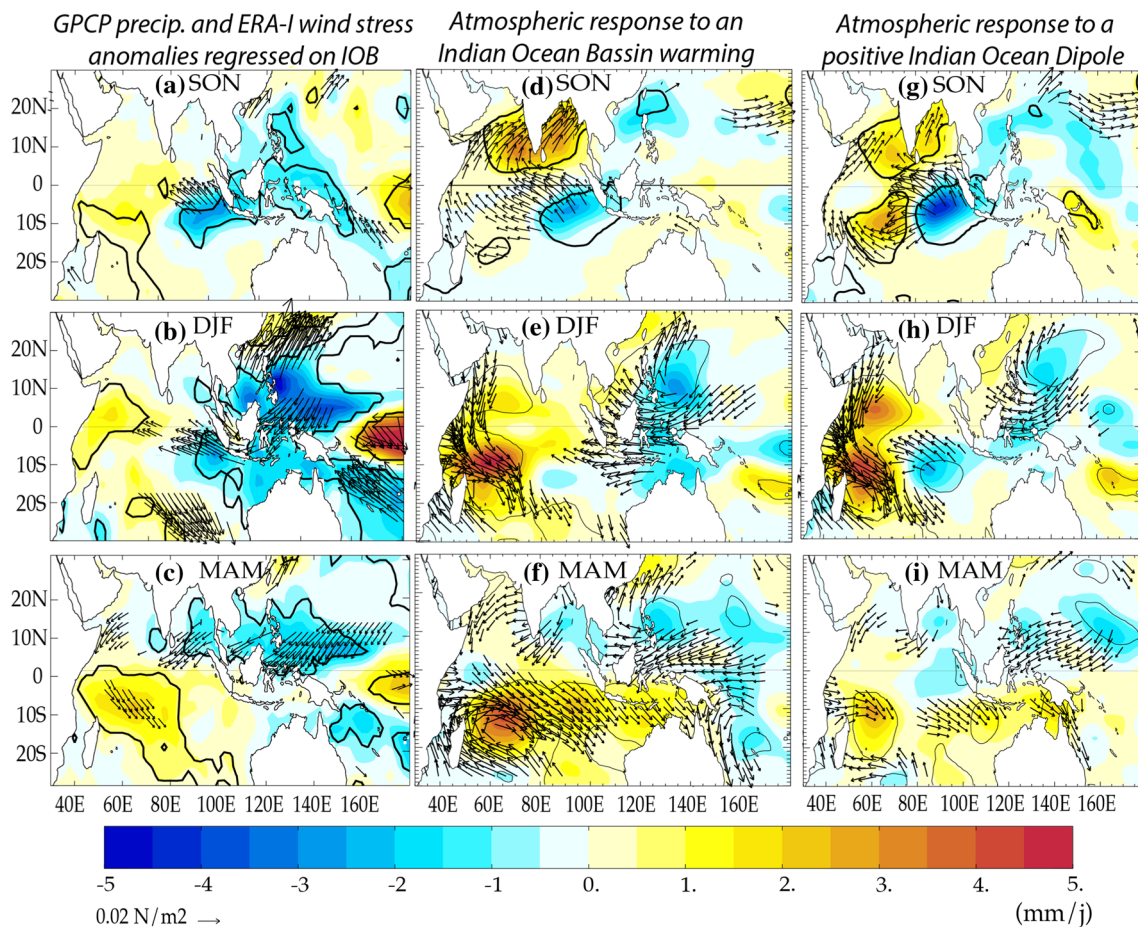


Fig. 11 GPCP precipitation (colours) and ERA-I winds stress (arrows) seasonal anomalies regressed onto the Indian-Ocean basin-wide warming (IOB) index for **a** SON, **b** DJF and **c** MAM. Precipitation (colours) and wind stress (arrows) seasonal anomalies ensemble mean in the **d**, **e**, **f** IOB and **g**, **h**, **i** IOD experiments during **d**, **g** SON,

e, **h** DJF and **f**, **i** MAM. Thick contours indicate precipitation anomalies that are significantly different from zero at the 95 % confidence level, and only wind stresses that are significantly different from zero at the 95 % confidence level are plotted

In the western tropical Pacific and maritime continent, a statistically significant negative precipitation anomaly develops in DJF, with an off-equatorial maximum in the Philippine Sea anticyclone. This is the manifestation of increased atmospheric subsidence, probably in response to a Walker circulation modulation through the positive deep convection anomalies that are locally forced over the entire Indian Ocean (Watanabe and Jin 2002). This negative deep-convection anomaly in the western Pacific reinforces the surface easterly response to the remote Indian Ocean warming, as expected from the Gill (1980) model. The tropical Indian Ocean warming persists during spring, most clearly in the IOB experiment (see Fig. 9j), further promoting enhanced deep convection in the Indian Ocean and a persistent easterly wind anomaly over the western Pacific (Fig. 11f). In both the IOD and IOB experiments, Indian Ocean SST anomalies induce a remote ZWSA over the western Pacific that occurs during boreal winter and spring

(i.e. during the Indian Ocean basin-wide warming) rather than during fall (i.e. rather than during the IOD peak). This ZWSA is also seen when regressing ERA-I wind stresses to the IOB index (Fig. 11h, i). Our sensitivity experiments are hence coherent with previous studies by Annamalai et al. (2005), Kug and Kang (2006) and Ohba and Ueda (2007) in terms of timing and sign of the wind anomalies. In contrast, they do not seem to confirm the mechanism suggested by Izumo et al. (2010), which rather emphasizes a westerly wind anomaly during the peak of the positive IOD.

Figure 12 finally illustrates the equatorial Pacific oceanic response to IOB and IOD ZWSA. As described above, the largest easterly wind stress perturbations occur in late boreal winter and early spring over the western Pacific, and then decrease. The easterly wind anomalies drive an upwelling Kelvin wave that reaches the central Pacific in January and the eastern Pacific in February in both cases. The downwelling Rossby wave generated by the easterly

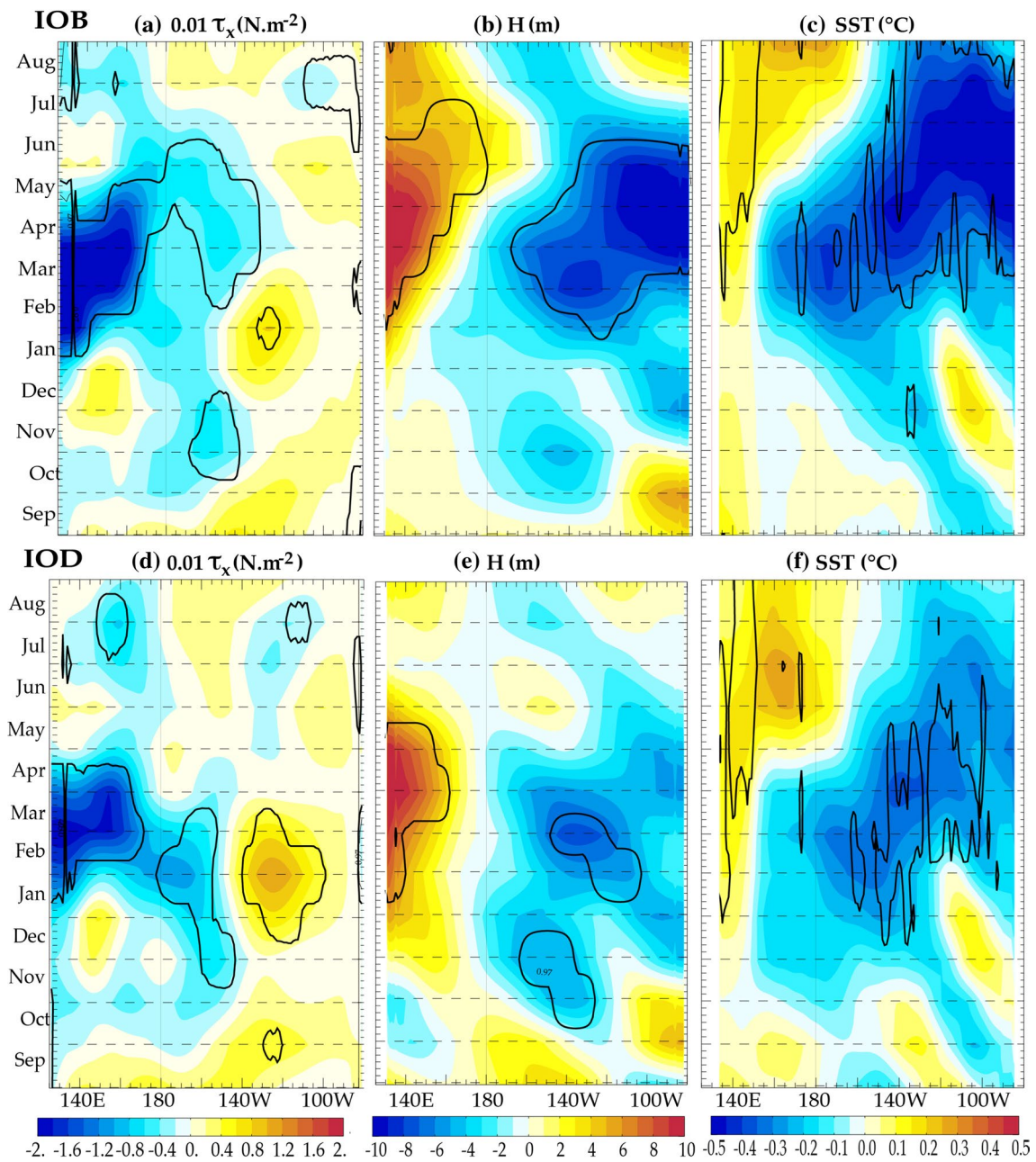


Fig. 12 Ensemble mean of the $3^{\circ}N$ – $3^{\circ}S$ average of **a** zonal wind stress anomalies in the IOB sensitivity experiment, **b** thermocline depth anomalies and **c** SST anomalies from the simple ocean model response to these wind stress anomalies. **c**, **d** The same fields, but

for the IOD sensitivity experiment. *Contours* indicate anomalies that are significantly different from the mean climatology (of the CLIM experiment) at the 95 % confidence level

anomaly is almost instantly reflected at the western boundary as a downwelling Kelvin wave, but this wave does not cancel out central Pacific upwelling anomalies due to the opposite effect of local easterly wind anomalies, that persist until April. The thermocline deepening (Fig. 12b) and easterly surface current anomalies (not shown) in the central Pacific progressively build up a negative SSTA in the Niño3.4 region, that peaks in March–April. These SST

anomalies appear to be larger and more significant for the IOB simulation as compared to the IOD one as a response to the larger and lasting-longer wind forcing. While these SST anomalies are just a few tenth of a degree in our experiments, they could be amplified by the Bjerknes feedback and tend to favour a transition to La Niña, as in Kug and Kang (2006), Ohba and Ueda (2007) and Izumo et al. (2010) scenarios.

5 Summary and discussions

5.1 Summary

This paper aims at identifying regions outside the tropical Pacific, which may influence ENSO through atmospheric teleconnections. We assume that ZWSA in the equatorial Pacific are a necessary condition to initiate or influence ENSO development. We hence use AGCM experiments to identify potential teleconnections between remote regions and zonal wind stresses in the western Pacific and a simple ocean model to translate these wind stresses in terms of oceanic response.

We have first run a 7-members ensemble AGCM experiment using climatological SST over the Pacific Ocean, and observed SST elsewhere over the 1982–2010 period. Even in the absence of SST interannual variability in the Pacific Ocean, the ensemble-mean of that experiment still displays a significant zonal wind stress variability in the western equatorial Pacific with maximum amplitude in boreal winter, driving a Niño3.4 SSTA response of ~ 0.5 °C. This SSTA response peaks in spring, and has a significant 0.35 lead correlation with the next ENSO peak, indicative of a potential weak influence of the remotely-forced wind anomalies on ENSO. The PACLIM ZWSA display significant correlation with SSTA in the tropical Indian Ocean, North and South Pacific, and North and tropical Atlantic Ocean.

Dedicated sensitivity experiments with typical SSTA patterns applied in each of these regions were then performed. We found that only the atmospheric response to Indian Ocean forcing displays statistically significant zonal wind stress and SST response (~ 0.3 °C in spring) in the equatorial Pacific. This suggests that, among the four tested regions, only SSTA in the Indian Ocean can induce a wind stress response over the tropical Pacific and influence ENSO in the AGCM used here. In addition, our results suggest that this potential influence of Indian Ocean SST anomalies on ENSO is due to the Indian Ocean Basin-wide mode maximum in DJF-MAM rather than the IOD mode in SON. Even if the influence of the Indian Ocean SST anomalies on ENSO is modest, it could be amplified by the Bjerknes feedback, particularly efficient in spring.

5.2 Discussion

A strong limitation of the present study lies in the forced framework employed that does not account for air–sea processes which have been suggested to play a key role in favouring the propagation of mid-latitude SST and wind anomaly into the tropics (e.g. Vimont et al. 2003; Terray 2010). Our study suggests that no direct teleconnection exists between mid-latitude SST anomalies and equatorial winds, but it does not preclude the coupled mechanism

proposed by Vimont et al. (2003) on the role of mid-latitude Pacific or by Ham et al. (2013) on the role of mid-latitude Atlantic on ENSO to operate. More experiments in a coupled framework are needed to test those hypotheses. Second, the two-tier approach of first deriving the equatorial Pacific wind stresses remotely forced from other regions, and then using them to force an ocean model effectively suppresses the Bjerknes feedback. It is hence difficult to know if the modest SST anomalies derived from the simple oceanic model would systematically evolve into an El Niño or not. In this respect, the studies of the effect of the tropical Atlantic on ENSO by Ding et al. (2012) and Martin-Rey et al. (2012), using a CGCM with full coupling over the Pacific and prescribed SST in the Atlantic is an interesting alternative to our two-tier approach.

There are also alternative methods for studying the effects of SST patterns external to the Pacific (e.g. Spencer et al. 2004), and for obtaining the SST patterns typical of various climate modes that we used in our short sensitivity experiments based on EOF analysis. Computing the SSTA patterns using other statistical methods, such as regressing SSTA on ENSO indices, generally results in similar spatial patterns and the particular methodology employed should not qualitatively affect the results discussed in the present study. The results of the present study are more likely to be affected by the atmospheric model used to perform the experiments. We did check that ECHAM5.4 was able to reproduce ENSO teleconnection patterns (Fig. 3), as well as reasonably reproduce the wind stress interannual variations in the western equatorial Pacific (correlation of 0.64) and wind and rainfall patterns forced by SSTA anomalies (Fig. 11). On the other hand, ECHAM displays much larger than observed equatorial wind stresses interannual variability there, in part due to the tendency to produce a large internal variability (~ 0.03 N m⁻², relatively to the observed ZWSA of ~ 0.015 N m⁻²). Furthermore, the atmospheric response to IOD-related SSTA seems underestimated by ECHAM in fall (Fig. 3). It is difficult to anticipate how these biases can affect our results, but enough to suggest testing the robustness of these results using other AGCMs.

The experiments presented in the present paper do not investigate the potential non-linearity of the atmospheric response to SST, and in particular the possible asymmetries between positive or negative SST anomalies. Such asymmetries can be expected, due to the non-linear nature of the deep atmospheric convection, that becomes sensitive to SST anomalies close to the 27.5 °C threshold (e.g. Graham and Barnett 1987). In particular, the coupled model analyses by Ohba and Watanabe (2012) show that, while basin-wide warm anomalies over the Indian Ocean tend to result in anomalous easterlies over the Pacific, and favour the transition to La Niña, such a mechanism does not occur in presence of cold anomalies over the Indian Ocean. We

did perform sensitivity experiments to investigate potential asymmetries in the AGCM response to a SST pattern associated with a positive or negative IOD (and following basin-wide warming or cooling). In partial agreement with Ohba and Watanabe (2012) analyses, our results do show some asymmetries in the AGCM response over the western Pacific, which are however not as strong as in their study (the response to IOB cooling is weaker, but still significant) and not strikingly statistically significant in our experimental setup. We have hence chosen not to include these results in the paper. More studies with different models and experimental contexts are hence probably needed to quantify the asymmetries of the western Pacific wind response to uniform SST anomalies over the Indian Ocean.

The present results are also not in line with the one presented in Dayan et al. (2013), which uses a statistical methodology to identify regions which bring additional predictability to the one intrinsic to the recharge-oscillator dynamics of the tropical Pacific. We found that the robust large-scale SST patterns, showing an influence on ENSO through an atmospheric teleconnection, are the Atlantic meridional mode and the South Pacific meridional mode in spring 3 seasons ahead, the southern Atlantic Ocean and the Indian Ocean Dipole, in fall 5 seasons ahead of the ENSO peak. These regions do not match the one of identified in the present study in which only the Indian Ocean can remotely influence ENSO in winter-spring. The analysis of Fig. 8 provides an indication of why it may be difficult to identify the influence of a teleconnection on ENSO from observations. A simple correlation analysis like Fig. 8 indeed points to almost all the regions that are influenced by ENSO as possible forcing regions for winds in the western Pacific, while the sensitivity experiments that are performed later allow to conclude otherwise that the Indian Ocean is the main forcing region.

Although our methodology points out the potential role of the Indian Ocean in modulating ENSO variability, it did not allow to clearly distinguish the respective influences of the IOD (Izumo et al. 2010) and of the following IOB basin-wide warming on the wind in the western Pacific (Annamalai et al. 2005) and ENSO (Kug and Kang 2006; Ohba and Ueda 2007). The fact that the largest wind perturbations occur in winter and spring, during the basin wide warming, however seem to confirm the studies that propose that the Indian ocean warming contributes to the phase transition of ENSO. Izumo et al. (2010) however emphasized that the fast decay of the IOD eastern pole induces fast variations of the wind stress in the western Pacific, that are more efficient for forcing an ocean response over the Tropical Pacific. This issue is currently under investigation and will be reported in a future study.

While the robustness of the present results must further be tested and the exact role of the Indian Ocean further

assessed, we think that the added value of our study is to investigate the potential teleconnections that influence ENSO globally, rather than focus on a particular region, as most previous studies (e.g. Vimont et al. 2001, 2003, 2009; Meehl et al. 2003; Clarke and Van Gorder 2003; Behera and Yamagata 2003; Annamalai et al. 2005; Kug and Kang 2006; Ohba and Ueda 2007; Rodríguez-Fonseca et al. 2009; Izumo et al. 2010, 2014; Ding et al. 2012; Martin-Rey et al. 2012). The only previous modelling studies that did compare the remote influence of several regions on ENSO (in that case the tropical Atlantic and Indian oceans) were performed by Jansen et al. (2009), using conceptual coupled models, and Frauen and Dommenges (2012), using a hybrid coupled model without ocean dynamics out of the tropical Pacific. We suggest that more studies that do compare the respective influences of SST in various regions on ENSO in a coupled multi-model context are needed.

Acknowledgments Hugo Dayan is funded by a PhD grant of Ministère de l'Enseignement Supérieur et de la Recherche and by the Institut National des Sciences de l'Univers (INSU) LEFE program. Jérôme Vialard, Takeshi Izumo and Matthieu Lengaigne are funded by Institut de Recherche pour le Développement (IRD). Sébastien Masson is funded by the Conseil National des Astronomes et Physiciens (CNAP). GPCP data are provided by the NOAA/OAR/ESRL PSD.

References

- Adler RF, Huffman GJ, Chang A, Ferraro R, Xie P-P, Janowiak J et al (2003) The version-2 global precipitation climatology project (GPCP) monthly precipitation analysis (1979–present). *J Hydro-meteorol* 4(6):1147–1167
- Alexander M, Vimont D (2010) The impact of extratropical atmospheric variability on ENSO: testing the seasonal footprinting mechanism using coupled model experiments. *J Clim* 2885–2901. doi:10.1175/2010JCLI3205.1
- Alexander MA, Bladé I, Newman M, Lanzante JR, Lau N-C, Scott JD (2002) The atmospheric bridge: the influence of ENSO teleconnections on air–sea interaction over the global oceans. *J Clim* 15(16):2205–2231
- Annamalai H, Xie SP, McCreary JP, Murtugudde R (2005) Impact of Indian Ocean sea surface temperature on developing El Niño*. *J Clim* 18:302–319
- Annamalai H, Kida S, Hafner J (2010) Potential impact of the tropical Indian Ocean–Indonesian Seas on El Niño characteristics. *J Clim* 23:3933–3952
- Behera SK, Yamagata T (2003) Influence of the Indian Ocean Dipole on the Southern Oscillation. *J Meteorol Soc Jpn* 81:169–177
- Bjerknes J (1969) Atmospheric teleconnections from the equatorial Pacific 1. *Mon Weather Rev* 97:163–172
- Boschat G, Terray P, Masson S (2013) Extratropical forcing of ENSO. *Geophys Res Lett* 40:1605–1611. doi:10.1002/grl.50229
- Burgers G (2005) The simplest ENSO recharge oscillator. *Geophys Res Lett* 32(13):L13706. doi:10.1029/2005GL022951
- Cai W, Qiu Y (2013) An observation-based assessment of nonlinear feedback processes associated with the Indian Ocean Dipole. *J Clim* 26:2880–2890
- Cavaleri DJ, Parkinson CL, Gloersen P, Comiso JC, Zwally HJ (1999) Deriving long-term time series of sea ice cover from

- satellite passive-microwave multisensor data sets. *J Geophys Res* 104(C7):15803. doi:[10.1029/1999JC900081](https://doi.org/10.1029/1999JC900081)
- Chang P, Ji L, Li H (1997) A decadal climate variation in the tropical Atlantic ocean from thermodynamic air–sea interactions. *Nature* 385:516–518
- Chiang JCH, Vimont DJ (2004) Analogous Pacific and Atlantic Meridional Modes of Tropical Atmosphere–ocean variability*. *J Clim* 17:4143–4158
- Clarke AJ, Van Gorder S (2003) Improving El Niño prediction using a space-time integration of Indo-Pacific winds and equatorial Pacific upper ocean heat content. *Geophys Res Lett* 30(7):1399. doi:[10.1029/2002GL016673](https://doi.org/10.1029/2002GL016673)
- Dayan H, Vialard J, Izumo T, Lengaigne M (2013) Does sea surface temperature outside the tropical Pacific contribute to enhanced ENSO predictability? *Clim Dyn*. doi:[10.1007/s00382-013-1946-y](https://doi.org/10.1007/s00382-013-1946-y)
- Dee DP, Uppala SM, Simmons AJ et al (2011) The ERA-interim reanalysis: configuration and performance of the data assimilation system. *Q J R Meteorol Soc* 137:553–597
- Deser C, Wallace JM (2003) Understanding the persistence of sea surface temperature anomalies in midlatitudes. *J Clim* 16:57–72
- Deser C, Alexander MA, Xie S-P, Phillips AS (2010) Sea surface temperature variability: patterns and mechanisms. *Annu Rev Mar Sci* 2:115–143. doi:[10.1146/annurev-marine-120408-151453](https://doi.org/10.1146/annurev-marine-120408-151453)
- Ding H, Keenlyside N, Latif M (2012) Impact of the equatorial Atlantic on the El Niño Southern Oscillation. *Clim Dyn* 38:1965–1972
- Du Y, Xie S-P, Huang G, Hu K (2009) Role of air–sea interaction in the long persistence of El Niño-induced North Indian Ocean Warming*. *J Clim* 22:2023–2038
- Federov AV, Brown JN (2009) Equatorial waves. In: Steele J (ed) *Encyclopedia of ocean sciences*, 2nd edn. Academic Press, New York, pp 3679–3695
- Fouquart Y, Bonnel B (1980) Computations of solar heating of the Earth's atmosphere: a new parameterization. *Beitr Phys Atm* 53:35–62
- Frankignoul C, Hasselmann K (1977) Stochastic climate models, part ii application to sea-surface temperature anomalies and thermocline variability. *Tellus* 29(4):289–305. doi:[10.1111/j.2153-3490.1977.tb00740.x](https://doi.org/10.1111/j.2153-3490.1977.tb00740.x)
- Frauen C, Dommengat D (2012) Influences of the tropical Indian and Atlantic Oceans on the predictability of ENSO. *Geophys Res Lett* 39:L02706. doi:[10.1029/2011GL050520](https://doi.org/10.1029/2011GL050520)
- Gill AE (1980) Some simple solutions for heat-induced tropical circulation. *Q J R Meteorol Soc* 106:447–462
- Glantz MH (2001) *Currents of change: El Niño's impact on climate and society*. Cambridge University Press, Cambridge
- Graham NE, Barnett TP (1987) Sea surface temperature, surface wind divergence, and convection over tropical oceans. *Science (New York, NY)* 238(4827):657–659. doi:[10.1126/science.238.4827.657](https://doi.org/10.1126/science.238.4827.657)
- Ham Y-G, Kug J-S, Park J-Y, Jin F-F (2013) Sea surface temperature in the north tropical Atlantic as a trigger for El Niño/Southern Oscillation events. *Nat Geosci* 6:112–116. doi:[10.1038/ngeo1686](https://doi.org/10.1038/ngeo1686)
- Horel JD, Wallace JM (1981) Planetary-scale atmospheric phenomena associated with the southern oscillation. *Mon Weather Rev* 109(4):813–829
- Izumo T, Vialard J, Lengaigne M, de Boyer Montegut C, Behera SK, Luo JJ, Cravatte S, Masson S, Yamagata T (2010) Influence of the state of the Indian Ocean Dipole on the following year's El Niño. *Nat Geosci* 3:168–172. doi:[10.1038/ngeo760](https://doi.org/10.1038/ngeo760)
- Izumo T, Lengaigne M, Vialard J, Luo J-J, Yamagata T, Madec G (2014) Influence of Indian Ocean Dipole and Pacific recharge on following year's El Niño: interdecadal robustness. *Clim Dyn* 42(1–2):291–310
- Jansen MF, Dommengat D, Keenlyside N (2009) Tropical atmosphere–ocean interactions in a conceptual framework. *J Clim* 22:550–567
- Klein SA, Soden BJ, Lau N-C (1999) Remote sea surface temperature variations during ENSO: evidence for a tropical atmospheric bridge. *J Clim* 12:917–932
- Kug J-S, Kang I-S (2006) Interactive feedback between the Indian Ocean and ENSO. *J Clim* 19:1784–1801
- Lohmann U, Roeckner E (1996) Design and performance of a new cloud microphysics parameterization developed for the ECHAM4 general circulation model. *Clim Dyn* 12:557–572
- Losada T, Rodríguez-Fonseca B, Polo I, Janicot S, Gervois S, Chauvin F, Ruti P (2010) Tropical response to the Atlantic equatorial mode: AGCM multimodel approach. *Clim Dyn* 5:45–52
- Martin-Rey M, Polo I, Rodríguez-Fonseca B, Kucharski F (2012) Changes in the interannual variability of the tropical Pacific as a response to an equatorial Atlantic forcing. *Scientia Marina* 76(S1):2012. doi:[10.3989/scimar.03610.19A](https://doi.org/10.3989/scimar.03610.19A)
- McCreary J (1976) Eastern tropical ocean response to changing wind systems: with application to El Niño. *J Phys Oceanogr* 6:632–645
- McGregor S, Holbrook NJ, Power SB (2009) The response of a stochastically forced ENSO model to observed off-equatorial wind-stress forcing. *J Clim* 22:2512–2525
- McPhaden MJ, Zebiak SE, Glantz MH (2006) ENSO as an integrating concept in earth science. *Science (New York, NY)* 314:1740–1745
- Meehl GA, Arblaster JM, Loschnigg J (2003) Coupled ocean–atmosphere dynamical processes in the tropical Indian and Pacific Oceans and the TBO. *J Clim* 16:2138–2158
- Mlawer EJ, Taubman SJ, Brown PD, Iacono MJ, Clough SA (1997) Radiative transfer for inhomogeneous atmospheres: RRTM, a validated k-correlated model for the longwave. *J Geophys Res* 102:16663–16682
- Murtugudde R, McCreary JP, Busalacchi AJ (2000) Oceanic processes associated with anomalous events in the Indian Ocean with relevance to 1997–1998. *J Geophys Res* 105:3295–3306
- Newman M, Compo G, Alexander MA (2003) ENSO-forced variability of the Pacific Decadal Oscillation. *J Clim* 16:3853–3857
- Niiler PP, Kraus EB (1977) One-dimensional models of the upper ocean. In: Kraus EB (ed) *Modeling and prediction of the upper layers of the ocean*. Pergamon Press, New York, pp 143–172
- Nobre P, Shukla J (1996) Variations of sea surface temperature, wind stress, and rainfall over the tropical Atlantic and South America. *J Clim* 9:2464–2479
- Nordeng TE (1994) Extended versions of the convective parameterization scheme at ECMWF and their impact on the mean and transient activity of the model in the tropics. *ECMWF Tech Memo* 206, 41 pp
- Ohba M, Ueda H (2005) Basin-wide warming in the equatorial Indian Ocean associated with El Niño. *SOLA* 1:89–92. doi:[10.2151/sola.2005-024](https://doi.org/10.2151/sola.2005-024)
- Ohba M, Ueda H (2007) An impact of SST anomalies in the Indian Ocean in acceleration of the El Niño to La Niña transition. *J Meteorol Soc Jpn* 85:335–348
- Ohba M, Watanabe M (2012) Role of the Indo-Pacific interbasin coupling in predicting asymmetric ENSO transition and duration. *J Clim* 25(9):3321–3335
- Picaut J, Ioualalen M, Menkes C, Delcroix T, McPhaden MJ (1996) Mechanism of the zonal displacements of the Pacific warm pool: implications for ENSO. *Science* 274(5292):1486–1489. doi:[10.1126/science.274.5292.1486](https://doi.org/10.1126/science.274.5292.1486)
- Reverdin G, Cadet D, Gutzler D (1986) Interannual displacements of convection and surface circulation over the equatorial Indian Ocean. *Q J R Meteorol Soc* 112:43–46
- Reynolds RW, Smith TM, Liu C, Chelton DB, Casey KS, Schlax MG (2007) Daily high-resolution-blended analyses for sea surface temperature. *J Clim* 20(22):5473–5496. doi:[10.1175/2007JCLI1824.1](https://doi.org/10.1175/2007JCLI1824.1)

- Rodríguez-Fonseca B, Polo I, García-Serrano J et al (2009) Are Atlantic Niños enhancing Pacific ENSO events in recent decades? *Geophys Res Lett* 36:L20705
- Roeckner E et al (2003) The atmospheric general circulation model ECHAM5. Part I: model description. Max Planck Institute for Meteorology Rep. 349, 127 pp
- Roeckner E, Brokopf R, Esch M, Giorgetta M, Hagemann S, Kornbluh L, Manzini E, Schlese U, Schulzweida U (2004) The atmospheric general circulation model ECHAM 5. PART II: sensitivity of simulated climate to horizontal and vertical resolution. MPI Report No. 354, Max Planck Institute for Meteorology, Hamburg
- Saji NH, Goswami BN, Viayachandran PN, Yamagata T (1999) A dipole mode in the tropical Indian Ocean. *Nature* 401:360–363
- Schulz J-P, Dümenil L, Polcher J (2001) On the land surface–atmosphere coupling and its impact in a single-column atmosphere model. *J Appl Meteorol* 40:642–663
- Simmons AJ, Burridge DM, Jarraud M, Girard C, Wergen W (1989) The ECMWF medium-range prediction models development of the numerical formulations and the impact of increased resolution. *Meteorol Atmos Phys* 40(1–3):28–60. doi:10.1007/BF01027467
- Spencer H (2004) Role of the atmosphere in seasonal phase locking of El Niño. *Geophys Res Lett* 31:L24104. doi:10.1029/2004GL021619
- Spencer H, Slingo JM, Davey MK (2004) Seasonal predictability of ENSO teleconnections: the role of the remote ocean response. *Clim Dyn* 22:511–526
- Terray P (2010) Southern Hemisphere extra-tropical forcing: a new paradigm for El Niño–Southern Oscillation. *Clim Dyn* 36:2171–2199
- Tiedtke M (1989) A comprehensive mass flux scheme for cumulus parameterization in large-scale models. *Mon Weather Rev* 117(8):1779–1800
- Tompkins AM (2002) A prognostic parameterization for the subgrid-scale variability of water vapor and clouds in large-scale models and its use to diagnose cloud cover. *J Atmos Sci* 59:1917–1942
- Trenberth KE, Hurrell JW (1994) Decadal atmosphere–ocean variations in the Pacific. *Clim Dyn* 9(6):303–319. doi:10.1007/BF00204745
- Trenberth KE, Branstator GW, Karoly D, Kumar A, Lau N-C, Ropelewski C (1998) Progress during TOGA in understanding and modeling global teleconnections associated with tropical sea surface temperatures. *J Geophys Res* 103(C7):14291–14324. doi:10.1029/97JC01444
- Vialard J, Menkes C, Boulanger J-P, Delecluse P, Guilyardi E, McPhaden M (2001) A model study of the oceanic mechanisms affecting the equatorial SST during the 1997–98 El Niño. *J Phys Oceanogr* 31:1649–1675
- Vimont DJ, Battisti DS, Hirst AC (2001) Footprinting: a seasonal connection between the tropics and mid-latitudes. *Geophys Res Lett* 28:3923–3926
- Vimont DJ, Wallace JM, Battisti DS (2003) The seasonal footprinting mechanism in the Pacific: implications for ENSO*. *J Clim* 16:2668–2675
- Vimont DJ, Alexander M, Fontaine A (2009) Midlatitude excitation of tropical variability in the Pacific: the role of thermodynamic coupling and seasonality*. *J Clim* 22(3):518–534. doi:10.1175/2008JCLI2220.1
- Wallace JM, Gutzler DS (1981) Teleconnections in the geopotential height field during the Northern Hemisphere Winter. *Mon Weather Rev* 109(4):784–812
- Wang W, McPhaden MJ (2000) The surface-layer heat balance in the equatorial Pacific Ocean. Part II: interannual variability*. *J Phys Oceanogr* 30(11):2989–3008
- Watanabe M, Jin F-F (2002) Role of Indian Ocean warming in the development of the Philippine Sea anticyclone during El Niño. *Geophys Res Lett* 29. doi:10.1029/2001GL014318
- Webster PJ, Moore AM, Loschnigg JP, Leben RR (1999) Coupled oceanic–atmospheric dynamics in the Indian Ocean during 1997–98. *Nature* 401:356–360
- Wentz FJ, Gentemann C, Smith D, Chelton D (2000) Satellite measurements of sea-surface temperature through clouds. *Science* 288:847–850
- Wu R, Kirtman BP, Krishnamurthy V (2008) An asymmetric mode of tropical Indian Ocean rainfall variability in boreal spring. *J Geophys Res* 113:D05104. doi:10.1029/2007JD009316
- Xie S-P, Hu K, Hafner J et al (2009) Indian Ocean capacitor effect on Indo-Western Pacific climate during the summer following El Niño. *J Clim* 22:730–747
- Zebiak SE (1993) Air–sea interaction in the equatorial Atlantic region. *J Clim* 6:1567–1586
- Zebiak SE, Cane MA (1987) A model El Niño–Southern Oscillation. *Mon Weather Rev* 115:2262–2278
- Zhang H, Clement A, Di Nezio P (2014) The South Pacific Meridional Mode: a mechanism for ENSO-like variability. *J Clim* 27:769–783. doi:10.1175/JCLI-D-13-00082.1